



# Calibrating Tomo-e Gozen Photometry Using SDSS Stripe 82 Standard Stars

TF.Zhang (U.Tokyo) et al.



## 1. Introduction

This study aims to enhance the photometric accuracy of the Tomo-e Gozen camera using the SDSS Stripe 82 standard stars catalog provided by Ivezić et al. (2007).

Initially, we evaluate the influence of zero magnitude, measured using three different methods, on photometric accuracy. Subsequently, we assess the effect of varying aperture sizes and the use of SExtractor magauto on photometric accuracy. Finally, we will filter the data from different dimensions and try to establish an effective criterion for excluding outliers.

The catalog from Ivezić et al. (2007) contains 991,472 standard stars, of which 283,605 have sufficient brightness to be observed by Tomo-e Gozen. Our observations with Tomo-e Gozen span from MJD 58432 (November 10, 2018) to MJD 60527 (May 8, 2024), and Figure 1 displays the number of observational epochs for standard stars at different magnitudes.

## 2. Method

### 2.1 Zero Magnitude Determination

The Tomo-e Gozen camera has three different methods to determine zero magnitude. The first method involves measuring the zero magnitude of each frame using the r-band data from the Pan-STARRS catalog, the second method uses a linear combination of g, r, and i-band data from the Pan-STARRS catalog, and the third method employs G-band data from Gaia (E)DR3 for this purpose. The band passes for Tomo-e Gozen, the g, r, i bands of the Pan-STARRS catalog, and the G-band of Gaia (E)DR3 are shown in Figure 2.

Figure 3 presents the photometric uncertainties achieved using the three different methods, with the x-axis representing the g-band magnitude of standard stars from the SDSS catalog. We bin the standard stars based on their SDSS catalog g-band magnitude, with a bin width of 0.01 mag. For each standard star, we calculate the standard deviation in the unit of magnitude of repeat photometry (SExtractor magauto) using the three different zero magnitudes. For standard stars within the same bin, the median of the standard deviation is taken as the photometric uncertainties for that zero magnitude determination method at that certain binned magnitude.

From Figure 3, it is evident that the zero magnitude determined using Gaia G-band data performs best, followed by the linear combination of g, r, and i-band data from the Pan-STARRS catalog, with the zero magnitude determined using only Pan-STARRS catalog r-band data showing the least optimal performance. Notably, the two Pan-STARRS determined zero magnitudes, when combined with SExtractor magauto, perform worse in brighter end (16 magnitude or brighter) compared to fainter end and are also with a significant number of measurement failures (already excluded prior to plotting and not shown in the graph). Conversely, the photometric uncertainties of measurements determined using zero magnitudes from the Gaia catalog increase as the target become fainter as expected. Therefore, we will select the G-band data from Gaia (E)DR3 as our catalog for determining zero magnitude.

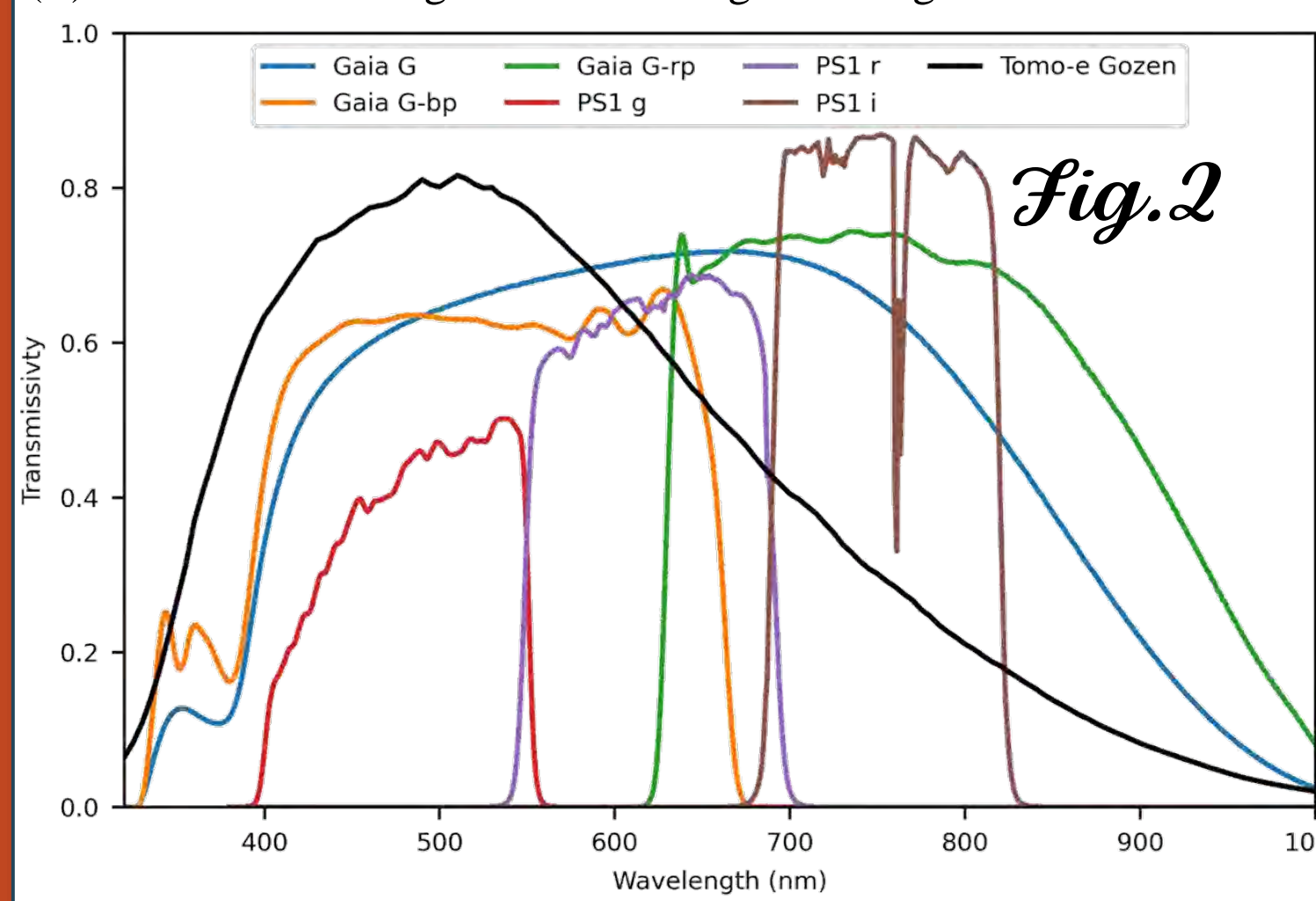


Fig. 2

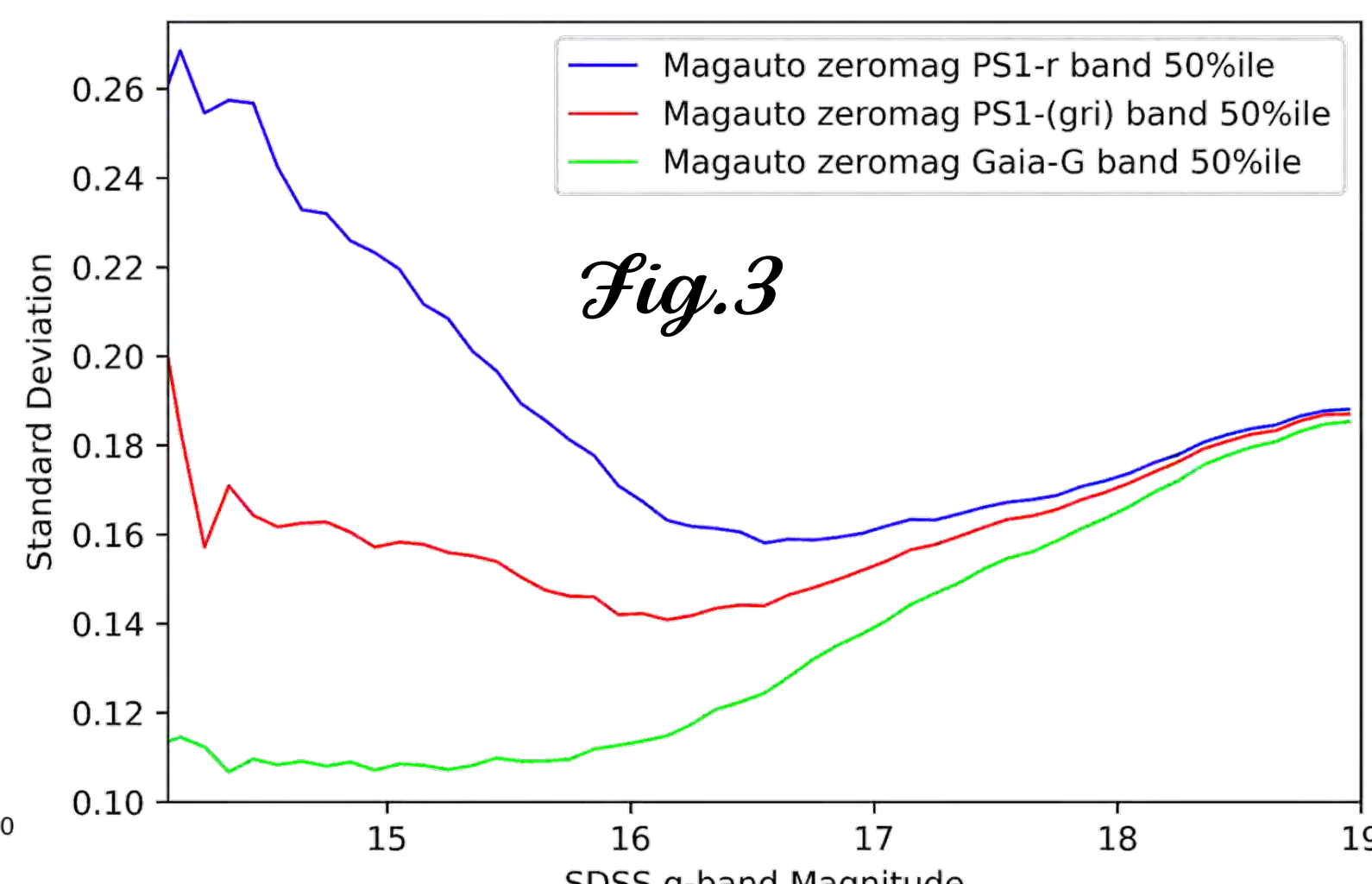


Fig. 3

### 2.2 Aperture Determination

Next, we will evaluate the advantages and disadvantages of magauto compared to fixed aperture photometry. Source Extractor magauto is an automated photometry method designed to optimally capture the total flux from target while minimizing background noise. Inspired by Kron's "first moment" algorithm, it determines an adaptive aperture based on the light distribution of each detected object. This aperture, called the Kron radius, is scaled by a factor to ensure that it encompasses most of the light from the source, ideally capturing 90% or more of the total flux. The performance of magauto heavily depends on the appropriate setting of parameters such as the scaling factor and the minimum aperture size, as well as the quality of the input image. Figure 4 shows the photometric uncertainties for data obtained using four different fixed apertures and magauto, all based on zero magnitudes determined from Gaia G-band.

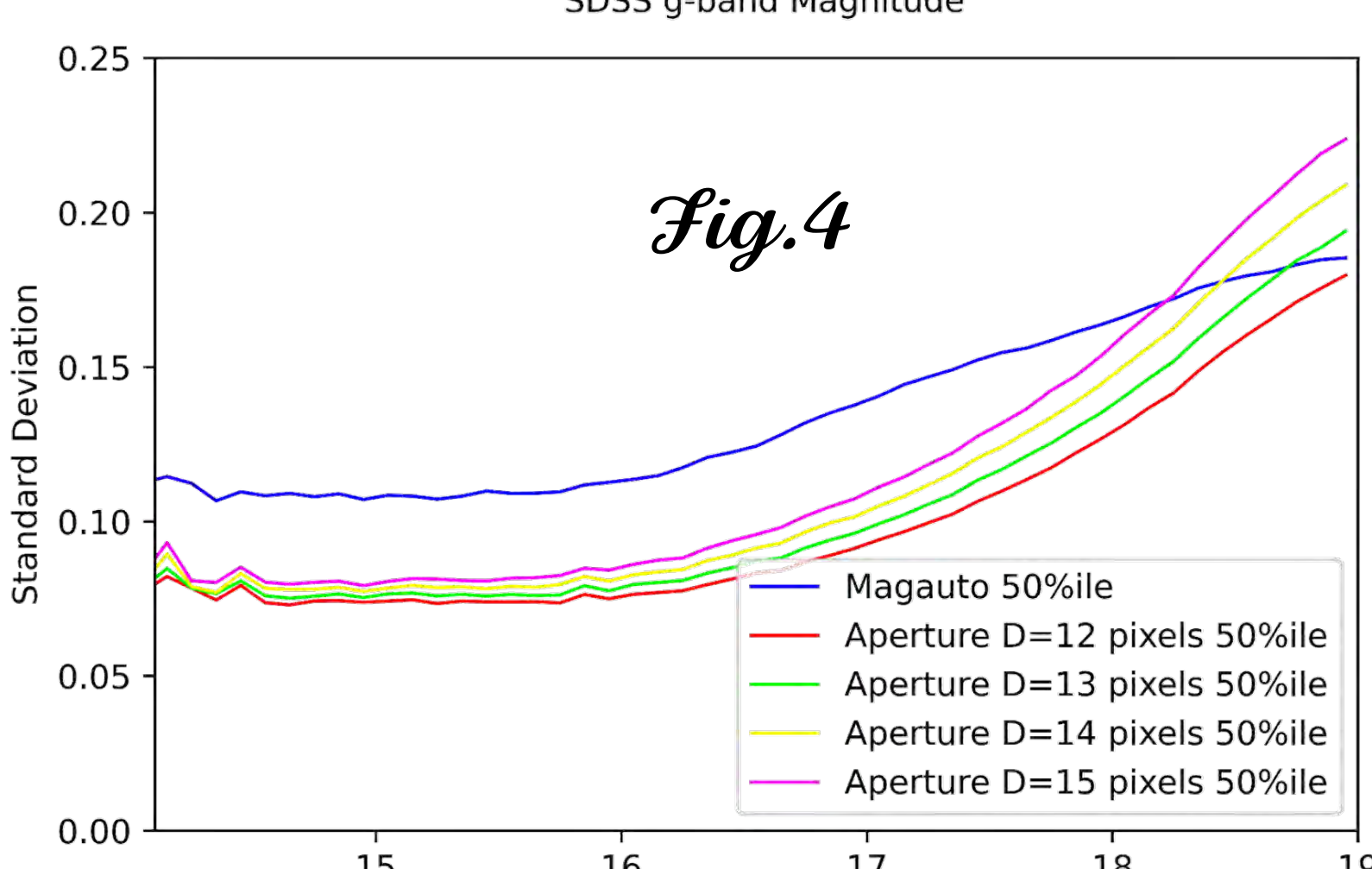


Fig. 4

The graph demonstrates that photometric uncertainties decrease as the fixed aperture size reduces, particularly at the fainter end. Magauto shows the poorest performance at the brighter end but outperforms all fixed apertures except for the 12-pixel diameter at the fainter end. However, fixed aperture photometry has the distinct advantage of allowing the selection of a zero magnitude using an aperture of the same size as the fixed aperture during measurements, which significantly reduced the photometric uncertainties, especially at the brighter end, and this is an advantage that magauto does not offer. Therefore, we will proceed with data filtering using a fixed aperture of 12 pixels in diameter combined with zero magnitudes determined by Gaia G-band.

### 2.3 Data Selection

In Section 2.3, we will filter the photometric data to exclude anomalies by considering several factors: the photometric center position, the date of observation, the full width at half maximum (FWHM) of the photometry, the number of sources in the same frame, and the zero magnitude value of the frame.

We first discuss the relative position of the photometric center within the frame. Each frame of Tomo-e Gozen measures 2000 pixels in width and 1128 pixels in height. Figure 5 illustrates the impact on photometric accuracy when the photometric center is close to the edge of the frame. It is evident from the figure that when the photometric center is less than 4 pixels from the frame edge, the photometric accuracy will decrease. This decrease occurs because part of the object lies outside the frame, leading to an underestimation of its magnitude. Therefore, we have decided to exclude all photometric measurements where the center is within 4 pixels of the frame edge. This means we will only retain measurements where the photometric center is positioned horizontally between 4 and 1124 pixels. Figure 6 displays the deviations of RA and Dec for the same standard star at different magnitudes across various epochs, with the y-axis showing the standard deviation of RA and Dec in degrees.

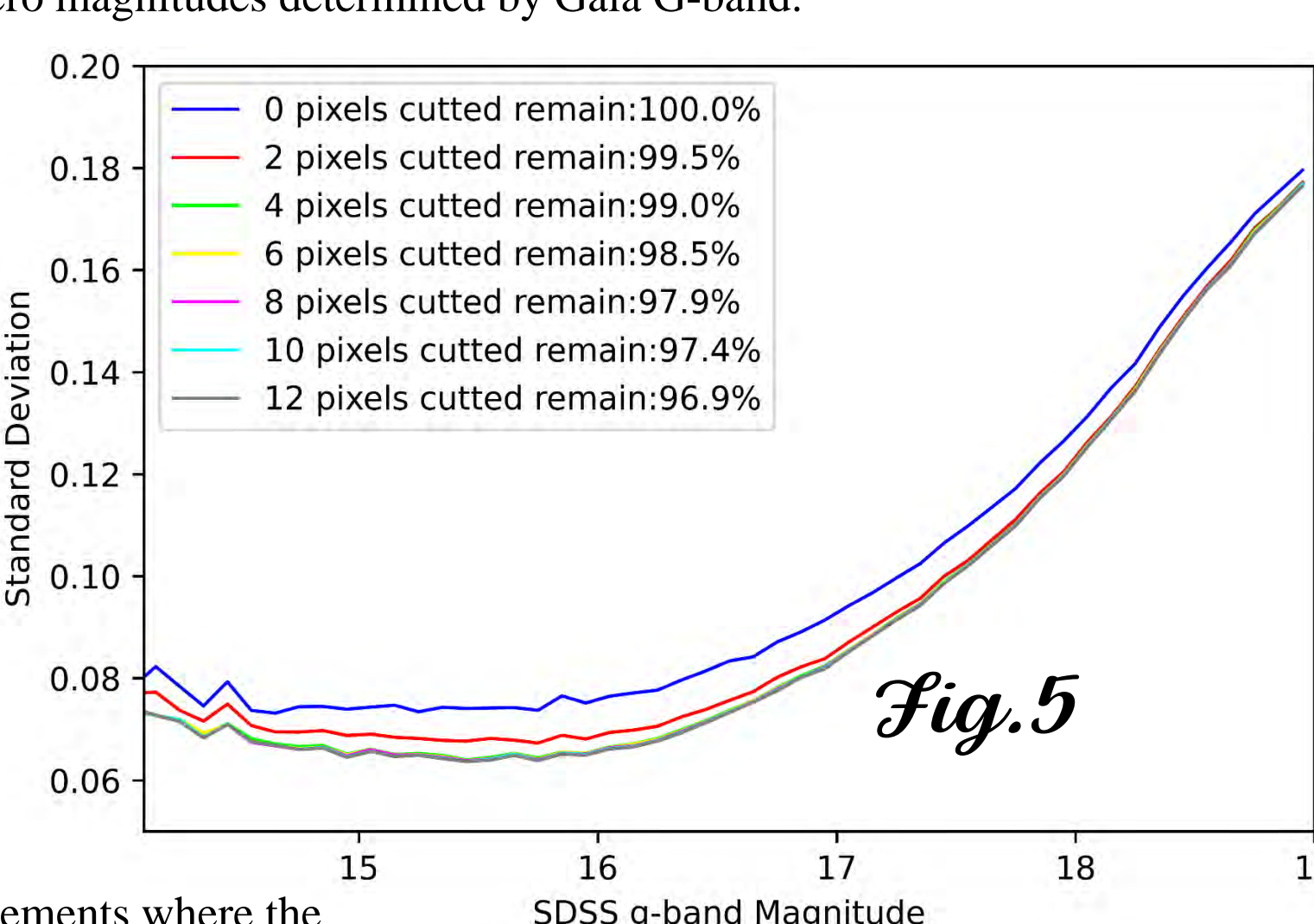


Fig. 5

The standard deviation in Dec increases with magnitude, whereas the standard deviation in RA initially decreases before increasing with rising magnitudes. Overall, RA standard deviations are higher than those in Dec. The reason causing higher uncertainties in RA, especially at the brighter end, have not yet been clearly identified but may be due to lesser precision of the telescope's azimuth axis compared to its altitude axis. Figure 7 shows the results of our data filtering based on RA and Dec. Deviations in the photometric center position are typically caused by poor seeing conditions or telescope vibrations. Excluding these biased values can reduce photometric uncertainties. The term '1% cutted' in the graph indicates that for any standard star's repeat photometry, we excluded values below the 1st percentile and above the 99th percentile for RA, and similarly for Dec. The 3% and 5% cuts represent the 3rd & 97th percentiles, and the 5th & 95th percentiles, respectively. As shown in the graph, photometric accuracy improves as the level of cuts increases, particularly at the brighter end. However, the data exclusion rate also rises sharply, and cuts above 1% at the fainter end do not further improve photometric accuracy.

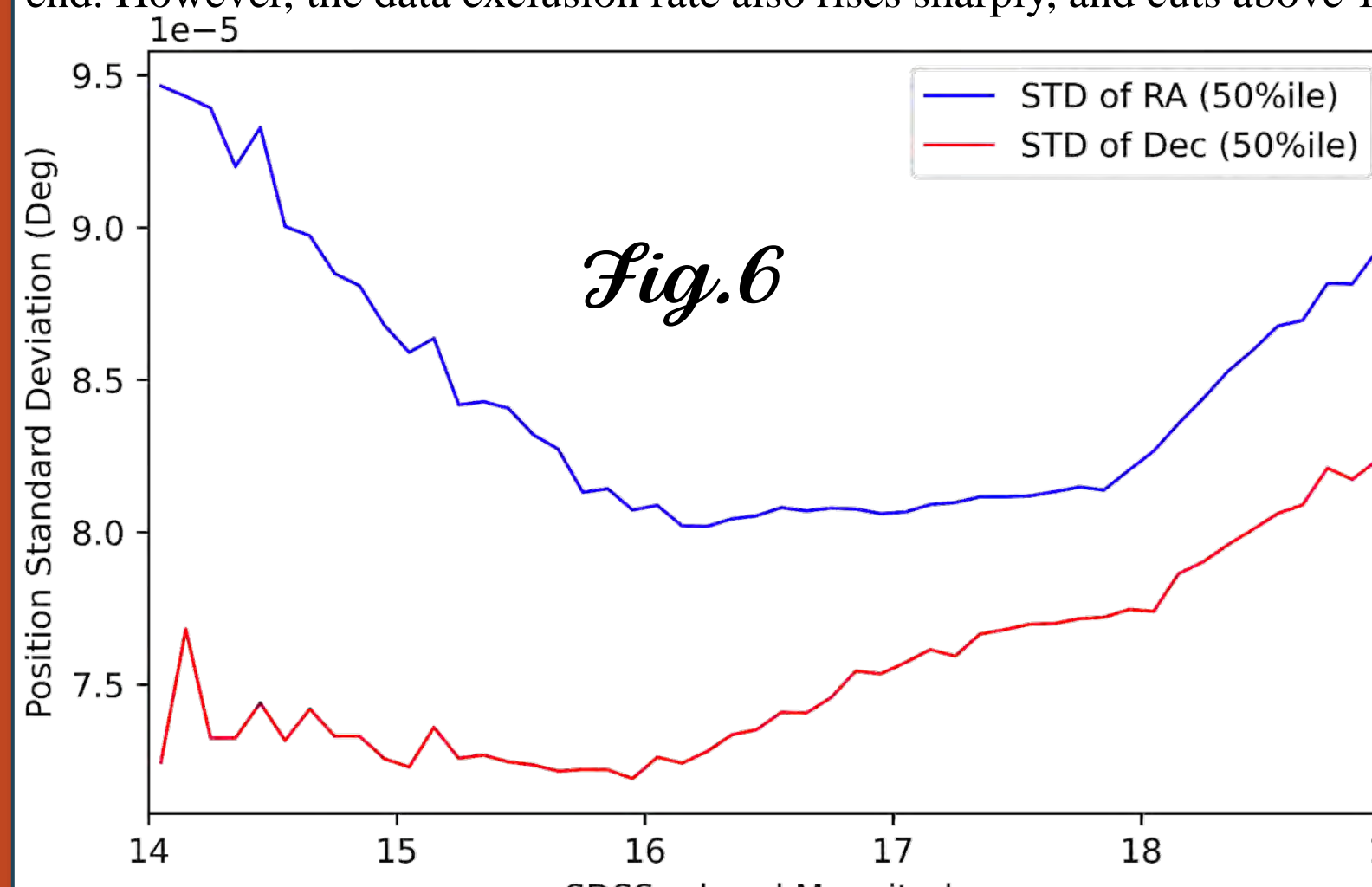


Fig. 6

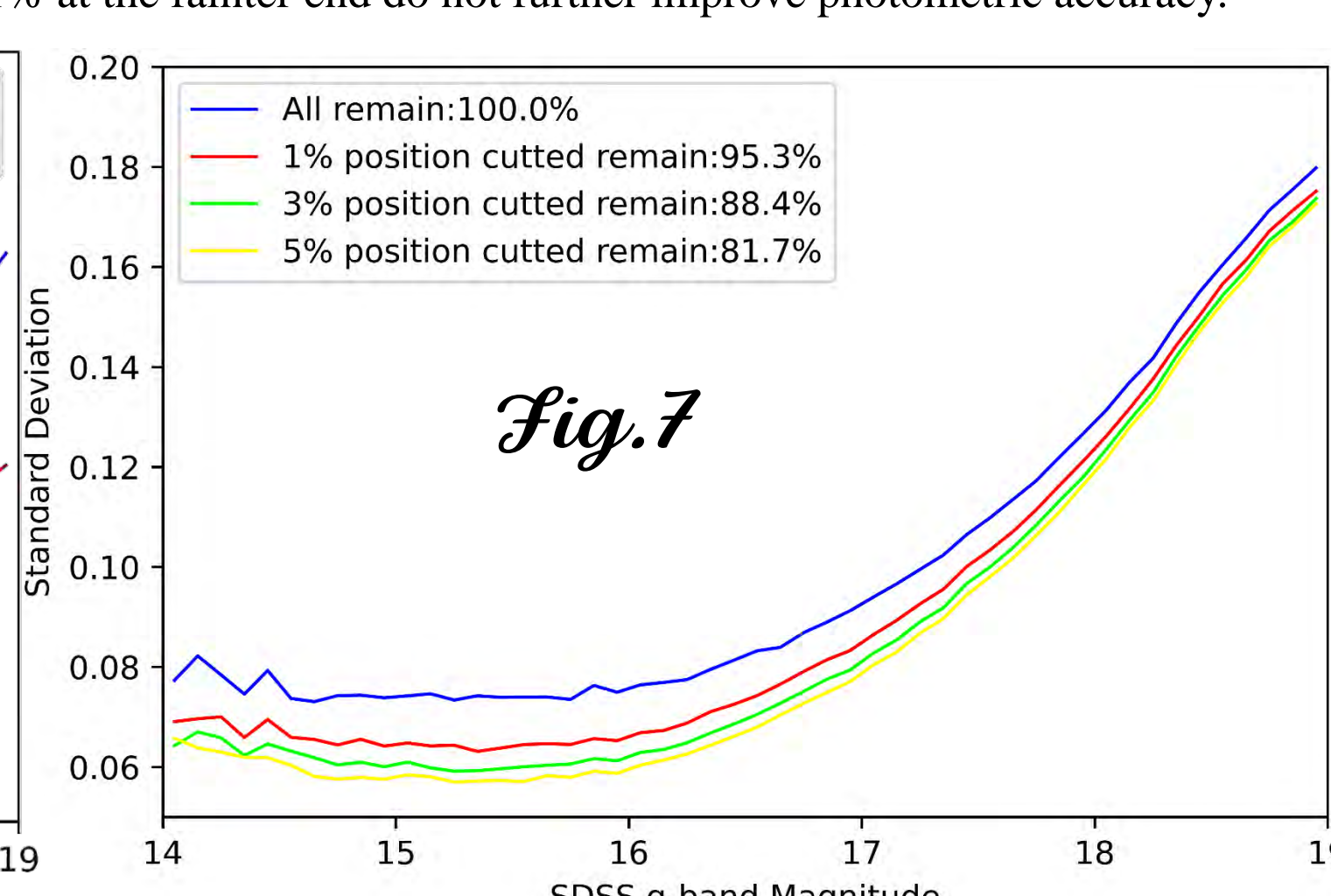


Fig. 7

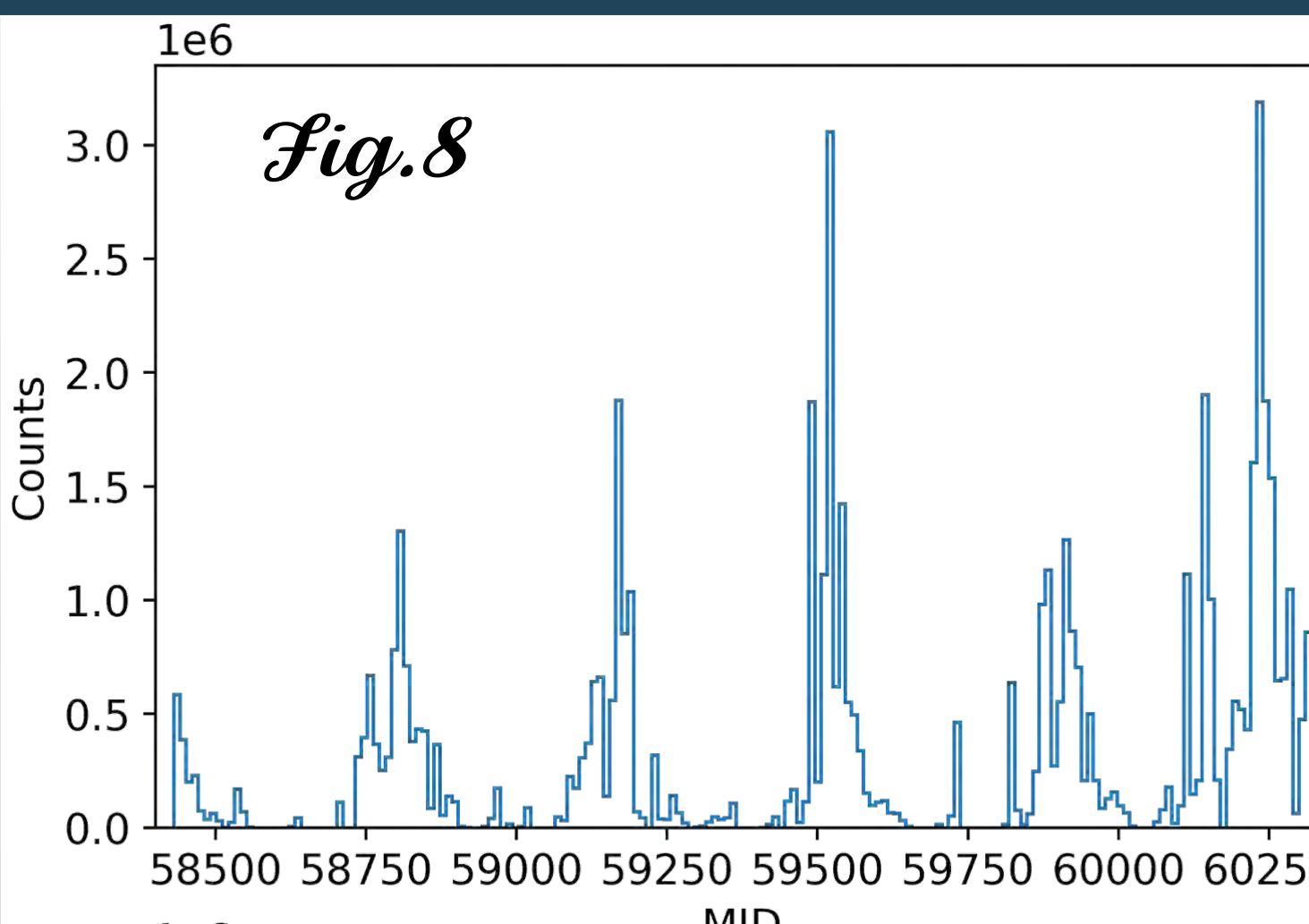


Fig. 8

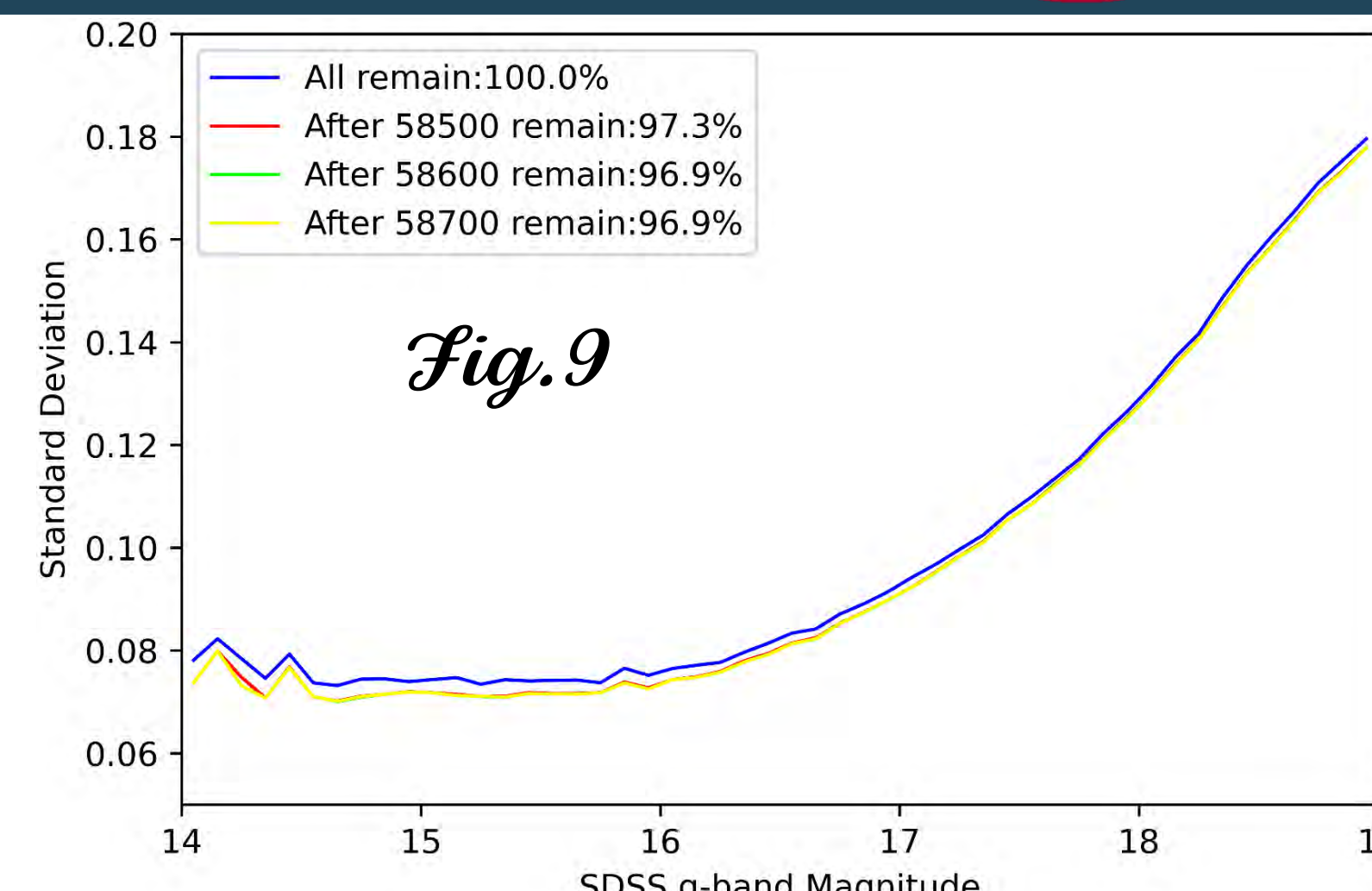


Fig. 9

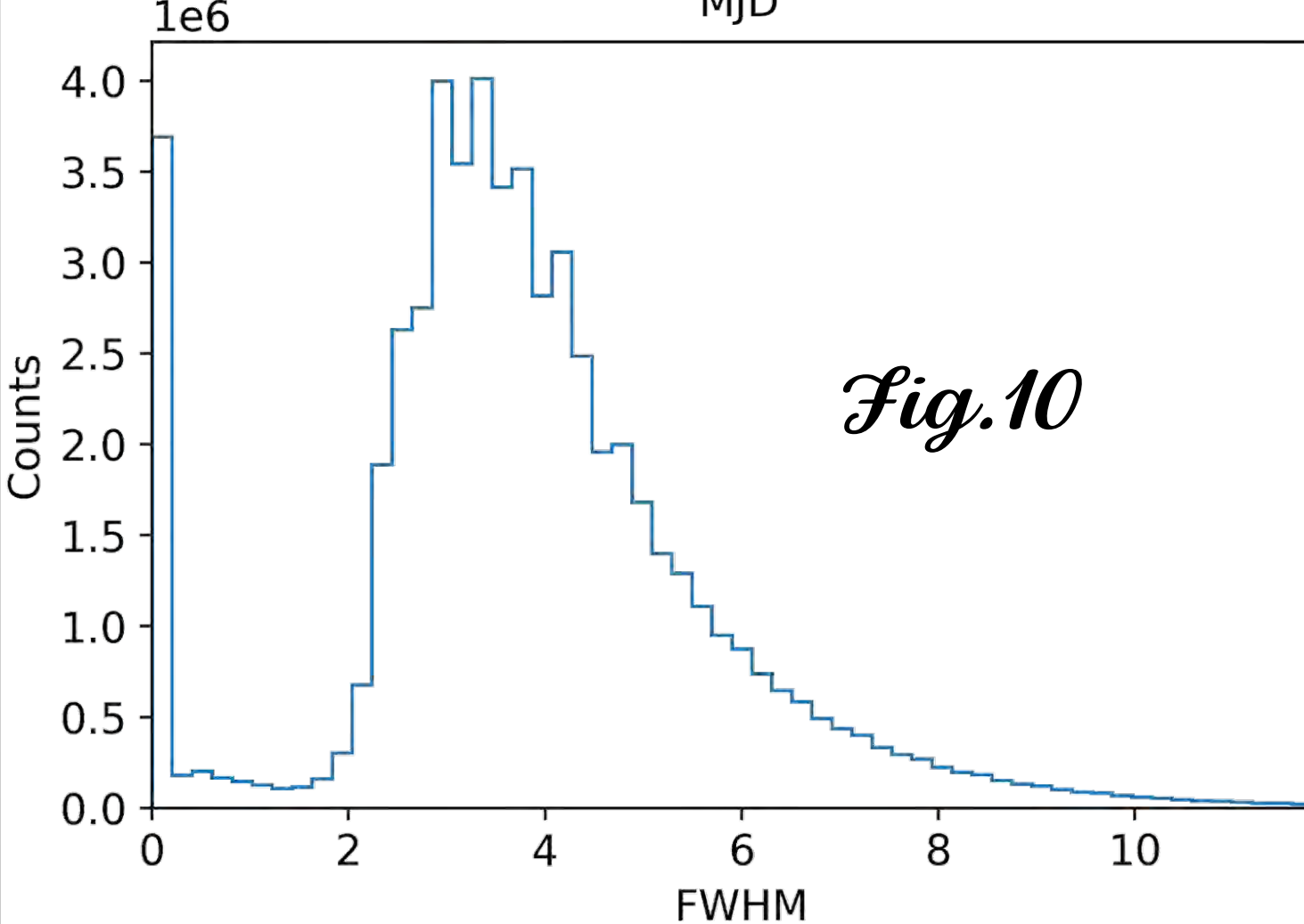


Fig. 10

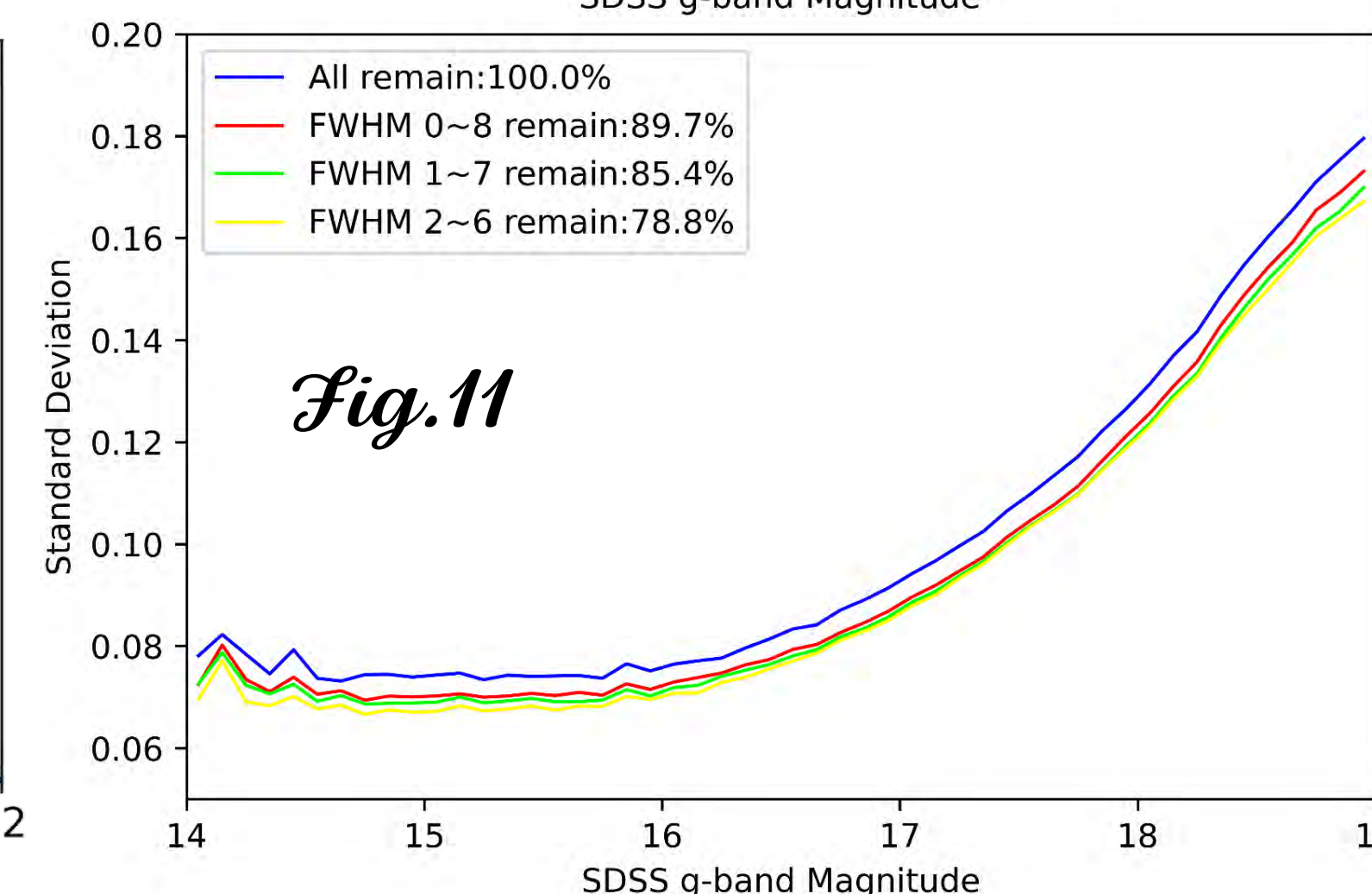


Fig. 11

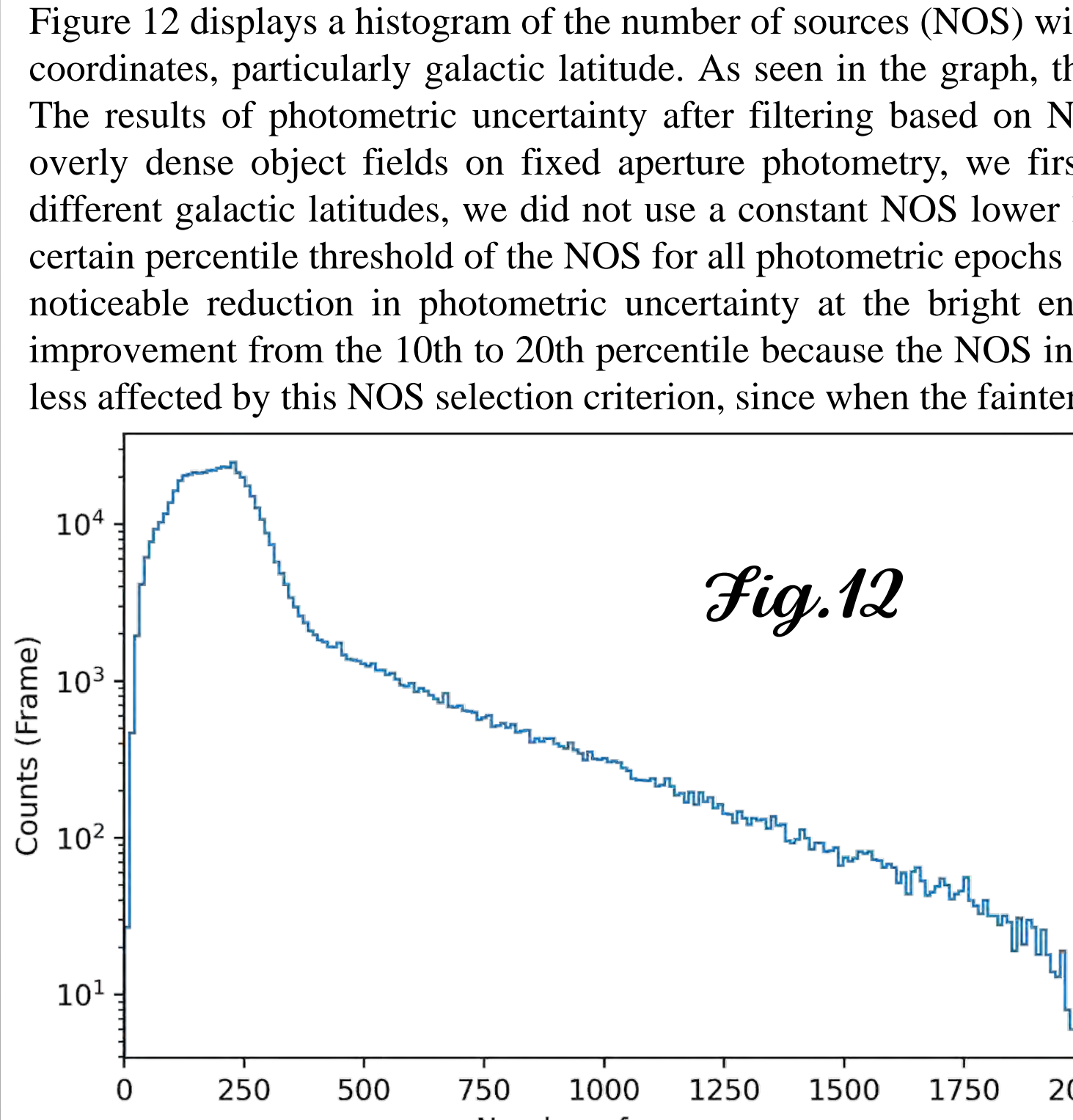


Fig. 12

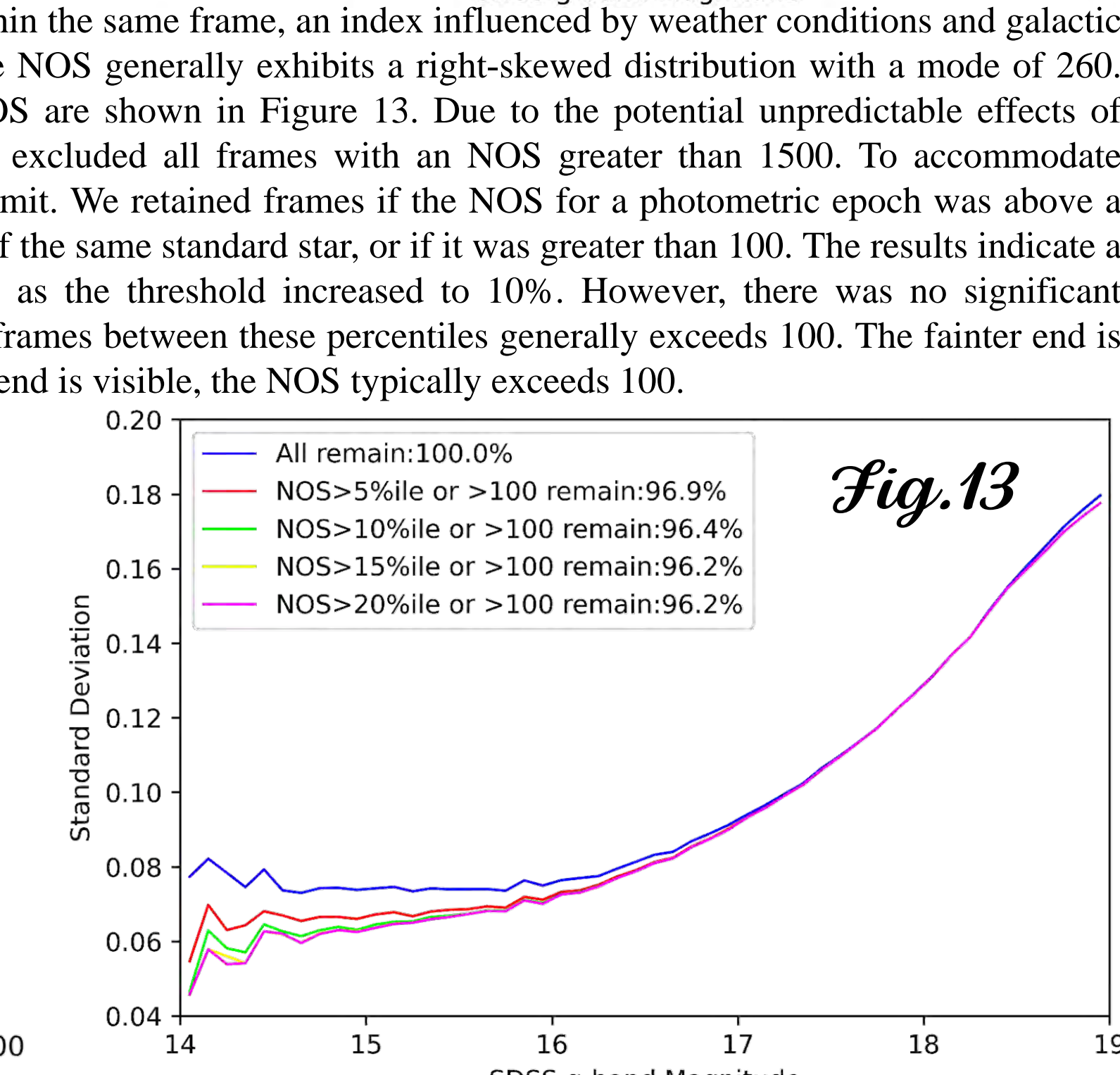


Fig. 13

Figure 14 shows a histogram of zero magnitudes for each frame, measured with a fixed 12-pixel aperture based on Gaia data, shown by the black line. The histogram displays a bimodal distribution with peaks at 25 and 25.5. This bimodality is due to the different positions of the CMOS sensors on the focal plane. To verify the relationship between focal plane position and zero magnitude distribution, we selected several detectors: Det 111 at the center, Det 116 on the north side, Det 416 on the south side, Det 141 on the west side, and Det 241 on the east side of the focal plane. Histograms of their zero magnitudes are also plotted in Figure 14. It is evident that CMOS at the focal plane central east-west axis have more observational epochs compared to those on the north and south sides, as Tomo-e Gozen's daily survey path is relatively fixed, Stripe 82 often spanning the telescope's focal plane from east to west. The three CMOS located along the central east-west axis exhibit negatively skewed distributions. The mode of zero magnitude distribution for Det 111 at the center is 25.5, while for Det 141 and Det 241, located on the east and west sides respectively, it is 25, indicating that the luminous flux at the focal plane center is superior to that on the sides. Given the differences in the position on the focal plane and luminous flux among the CMOS sensors, it is inappropriate to apply a uniform standard for filtering zero magnitudes across different CMOS. We calculated different percentiles for the zero magnitudes of each CMOS and filtered the data accordingly, as shown in Figure 15. After filtering, a reduction in photometric uncertainty is observed across all magnitudes, particularly at the brighter end, where removing data below the 5th percentile can halve the photometric uncertainty. This effect is less pronounced at the fainter end, as standard stars at the fainter end are usually not visible during poor weather (lower zero magnitudes). Increasing the filtering threshold can further reduce photometric uncertainty; however, beyond the 10th percentile, additional increases in the threshold show diminishing returns while significantly raise the data exclusion rate.

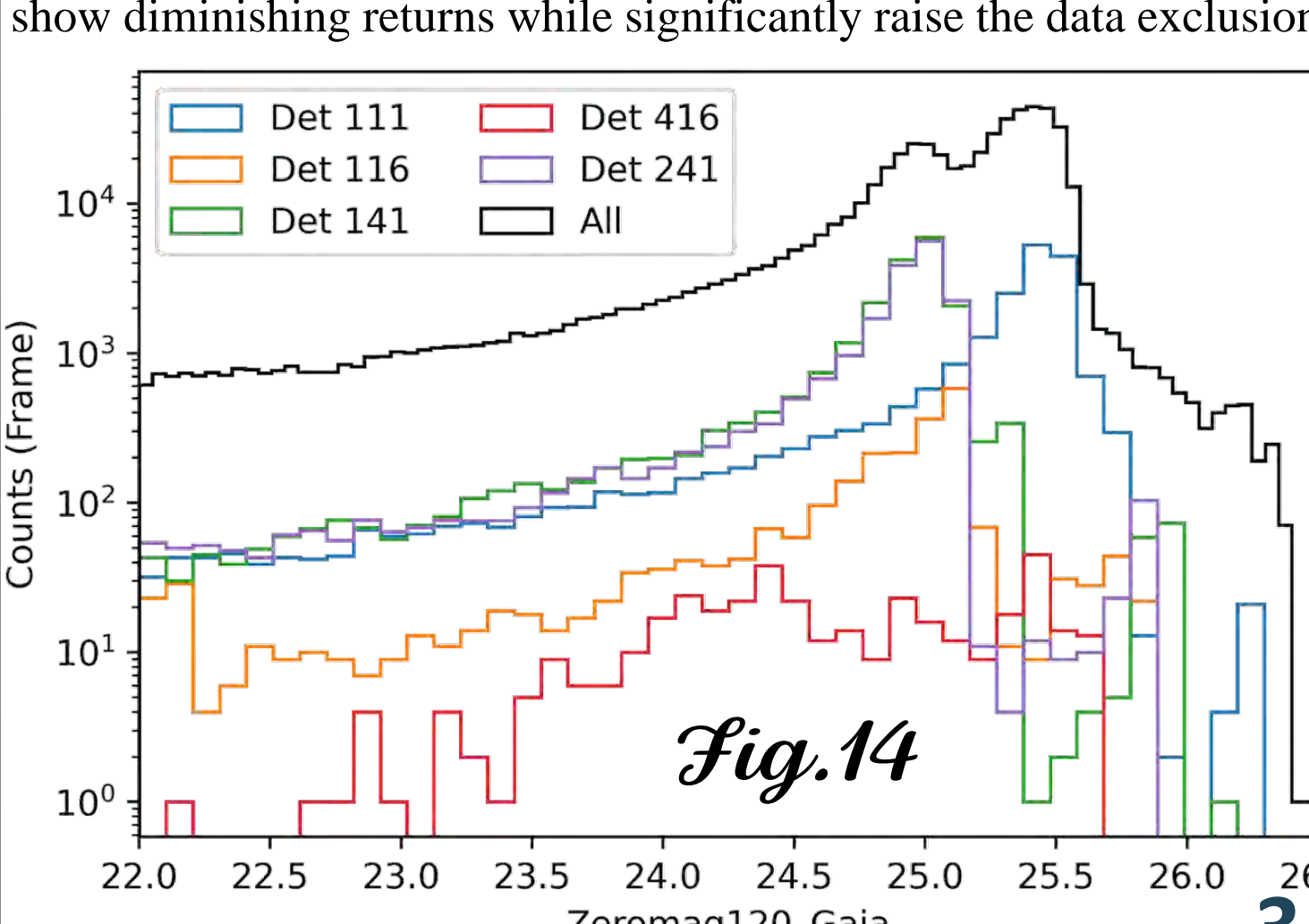


Fig. 14

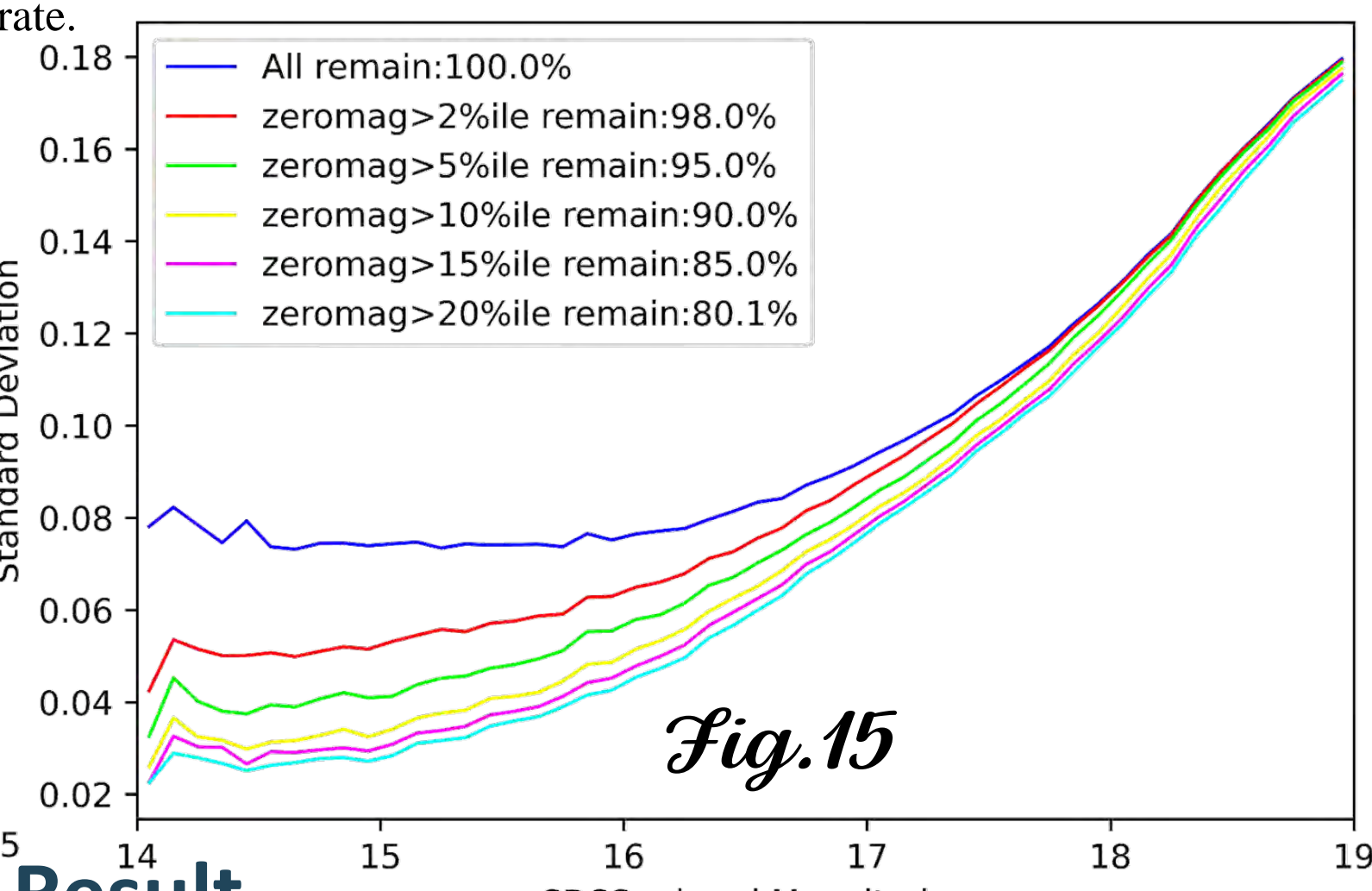


Fig. 15

## 3. Result

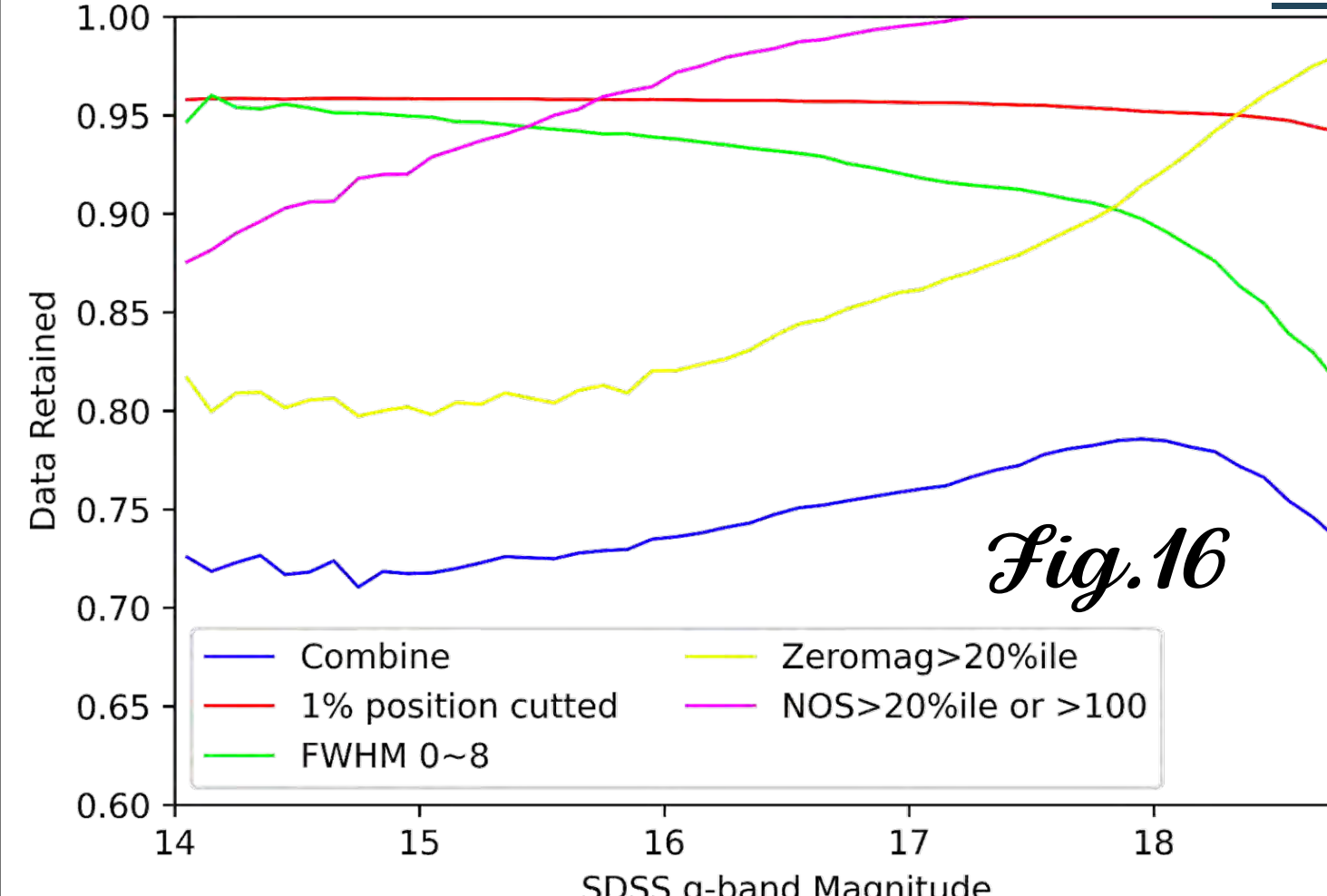


Fig. 16

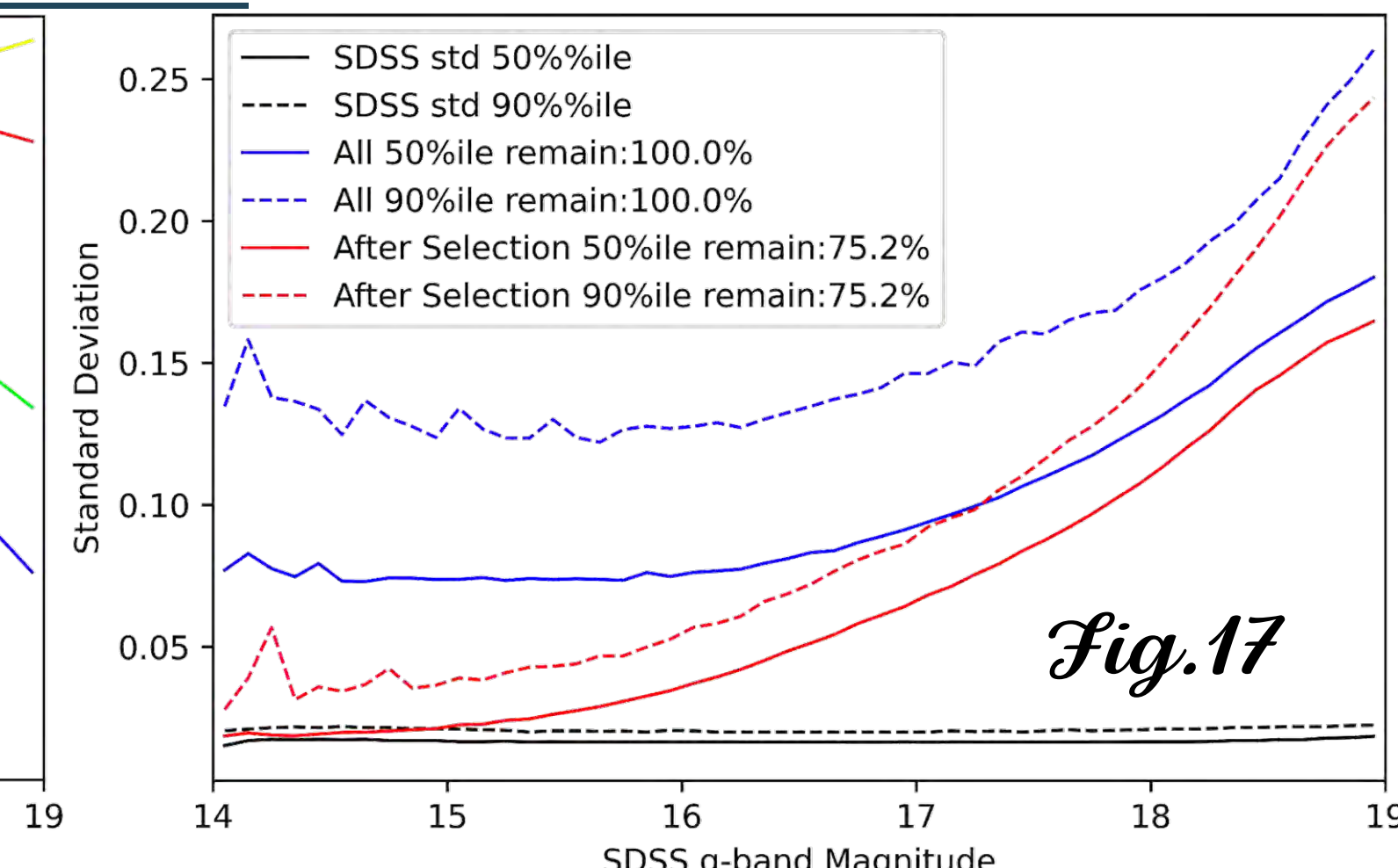


Fig. 17

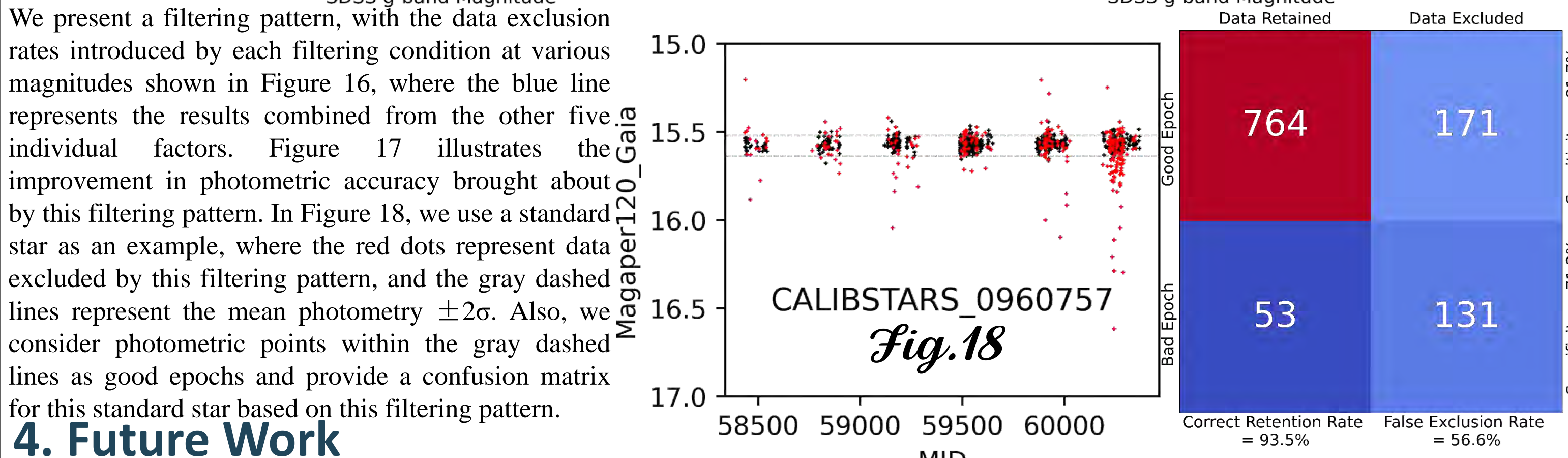


Fig. 18

## 4. Future Work

In our future work, we plan to undertake the following tasks: 1, In the measure.py script, we will compare the number of sources during zero magnitude determination with those in the same field of view from Gaia to select good frames. This comparison helps to avoid interference caused by varying star densities at different galactic latitudes. 2, We will broaden our analysis beyond Stripe 82 to more comprehensively assess CMOS zero magnitude, as the standard stars of Stripe 82 are rarely captured by the CMOS sensors at Tomo-e Gozen's northern and southern extremities, resulting in insufficient data for these sensors. 3, We plan to investigate the limitation magnitude of each frame to calculate the signal-to-noise ratio for each photometric measurement and explore how the signal-to-noise ratio affects photometric uncertainties. 4, We will conduct an in-depth analysis of the data that has been filtered out, attempting to identify any patterns in the deviations and explore potential corrections to enhance the data retention rate. 5, We propose to further reduce the existing aperture sizes (additionally measuring D=6, 7, 8, 9, 10, 11) to better quantify the fainter end, while maintaining the photometric accuracy at the bright end. 6, A zero magnitude determination method based on a linear combination of Gaia's dual-color (G-bp and G-rp) may prove superior to the current method that uses Gaia's monochrome data. These initiatives will guide our research efforts moving forward.

In Figure 8, we present a histogram of the observation dates for photometric epochs during the observation period. A clear seasonal trend is evident, which is attributed to the frequent rainfall in the Kiso area during summer, making it less suitable for astronomical observations. In contrast, winter generally allows for a large number of effective observations. Additionally, as shown in Figure 9, we also filtered data from the early operation period of the telescope. The results indicate that the data quality obtained during the first two months of observations is slightly lower compared to the data after MJD 58500. We compiled all photometric measurements into a histogram of the Full Width at Half Maximum (FWHM) as shown in Figure 9. Excluding the unmeasurable data points (marked as 0), the FWHM generally displays a right-skewed distribution with a mode around 3.5 pixels. The results of photometric uncertainty after filtering based on FWHM are presented in Figure 10. Unlike other filtering methods that only improve the photometric accuracy at the brighter end, filtering based on FWHM can enhance the photometric accuracy for all magnitudes to a certain extent. However, the degree of improvement approaches a limit as the filtering progresses.